NASA TECHNICAL REPORT

NASA TR R-235

INVESTIGATION OF THE DIVERGENCE CHARACTERISTICS OF DELTA-PLANFORM CANARD CONTROLS

by A. Gerald Rainey, Perry W. Hanson, and Dennis J. Martin

Langley Research Center
Langley Station, Hampton, Va.

NATIONAL AERONAUTICS AND SPACE ADMINISTRATION • WASHINGTON, D. C. • APRIL 1966

NASA TR R-235

INVESTIGATION OF THE DIVERGENCE CHARACTERISTICS OF DELTA-PLANFORM CANARD CONTROLS

By A. Gerald Rainey, Perry W. Hanson, and Dennis J. Martin

Langley Research Center
Langley Station, Hampton, Va.

NATIONAL AERONAUTICS AND SPACE ADMINISTRATION

For sale by the Clearinghouse for Federal Scientific and Technical Information
Springfield, Virginia 22151 – Price $0.50

INVESTIGATION OF THE DIVERGENCE CHARACTERISTICS OF DELTA-PLANFORM CANARD CONTROLS[1]

By A. Gerald Rainey, Perry W. Hanson,
and Dennis J. Martin
Langley Research Center

SUMMARY

21643 1

The static aeroelastic divergence characteristics of a delta-planform model of a canard control surface have been studied both analytically and experimentally in the Mach number range from 0.6 to 3.0. The experiments indicated that divergence occurred at a nearly constant value of dynamic pressure at Mach numbers up to 1.2. At higher Mach numbers somewhat higher values of dynamic pressure were required to produce divergence. The analysis and the experiment indicate that the camber stiffness of the control surface and the stiffness of the control actuator are both important in divergence of surfaces of this type.

Author 1

INTRODUCTION

Canard-type surfaces have potential application as stability and control devices for a wide range of aerospace vehicles. The increased usage of low-aspect-ratio canard surfaces for stability and control of missiles, launch vehicles, airplanes, target drones, and so forth, has led to considerable interest in the aeroelastic characteristics of such surfaces. In several instances, missile failures have occurred which were believed to be due to static aeroelastic divergence of surfaces of this type. In most cases, a relatively simple solution to the problem has been found such as stiffening the surface in the chordwise direction or altering the geometry of the control. Investigations of this type are usually somewhat restrictive and the results may not be generally available.

Divergence encountered by surfaces of this type differs somewhat from the classical torsional divergence in that camber deformations seem to play a dominant role. This new class of divergence problems which are associated with thin low-aspect-ratio surfaces has received some analytical study (refs. 1 and 2).

In order to assess this problem area further, an investigation of the effects of variations of stiffness and location of the pitch axis of this type of control surface has been undertaken. Divergence measurements have been made over the Mach number range from 0.6 to 3.0, and an analytical treatment of the divergence of this type of control has been developed. The structure has been treated as a beam with its span alined with the airstream. Two types of

---

[1]Supersedes recently declassified NACA RM L58E07 by A. Gerald Rainey, Perry W. Hanson, and Dennis J. Martin, 1958.

aerodynamic forces are considered, one based on very-low-aspect-ratio theory and the other based on piston theory. The experimental results are compared with the results of this analysis.

SYMBOLS

Measurements for this investigation were taken in the U.S. Customary System of Units. Equivalent values are indicated herein in the International System (SI) in the interest of promoting use of this system in future NASA reports. Conversion factors for the units used herein are presented in appendix A.

A_{ij} slope influence coefficient for panel, pitch spring being considered infinitely stiff (slope at position i due to unit load at position j)

a speed of sound

a_{ij} slope influence coefficient for pitch spring, panel being considered infinitely stiff

B_{ij} slope influence coefficient for panel-spring combination, $a_{ij} + A_{ij}$

b model semichord measured parallel to root chord at three-quarter semispan

C_β spring constant of pitch spring

c distance from intersection of leading edge and root chord to trailing edge

d measured deflection of control surface at a point 27.1 percent of root chord rearward of leading edge and at 50 percent of local span outboard of root chord due to a unit load at that point with pitch spring stiffness assumed infinite

E modulus of elasticity of panel

E_A modulus of elasticity of air

$E_{M,e}$ effective value of modulus of elasticity of material

EI panel bending stiffness with respect to pitch axis

h measured deflection of infinitely stiff control surface at a point 27.1 percent of root chord rearward of leading edge and at 50 percent of local span outboard of root chord due to a unit load at that point acting against pitch spring stiffness only

i,j identifying integers in matrix notation

K_e effective stiffness of panel-spring combination, $\frac{l}{d + h}$

l length of trailing edge

M Mach number

M_b bending moment

m_A mass of air contained in cone for which base diameter is equal to root chord and height is equal to span

m_e effective mass of panel, $\frac{K_e}{\omega^2}$

m_p mass of panel

n integer

P aerodynamic load

p static pressure

q dynamic pressure

s one-half the distance from leading edge to root chord measured parallel to pitch axis at chordwise station x

t thickness of panel

V stream velocity

w component of stream velocity normal to control surface

x chordwise distance measured from and perpendicular to pitch axis (for analytical purposes, pitch axis is assumed perpendicular to line bisecting angle formed by leading edge and root chord)

x_i chordwise station where deflection is measured due to load at x_j

x_j chordwise station where load is placed

x_p distance of panel elastic axis from leading edge at root chord

z vertical displacement

γ ratio of specific heats

θ angle between leading edge and free-stream flow

μ mass ratio, $\frac{m_p}{m_A}$

ρ density of air

ω circular natural frequency of vibration

δ_{ij} $\begin{cases} = 1 & \text{if } i = j \\ = 0 & \text{if } i \neq j \end{cases}$

$[D]$ differentiating matrix

$[\ ]$ square matrix

$\{\ \}$ column matrix

Subscripts:

L refers to lower surface

U refers to upper surface

∞ refers to conditions far removed from control surface

Dots over symbols denote derivatives with respect to time.

APPARATUS AND TESTS

Description of Wind Tunnels

The tests were conducted in the Langley 2-foot transonic flutter tunnel for the Mach number range from 0.6 to 1.2 and in the Langley 9- by 18-inch supersonic flutter tunnel for the Mach number range from 1.64 to 3.0.

The Langley 2-foot transonic flutter tunnel is a slotted-throat single-return wind tunnel equipped to use either air or Freon-12 as a test medium. The present tests were made with Freon-12. The tunnel is of the continuous-operation type, powered by a motor-driven fan. Both test-section Mach number and density are continuously controllable.

The Langley 9- by 18-inch supersonic flutter tunnel is a fixed-nozzle blowdown-type wind tunnel exhausting into a vacuum sphere. The nozzle configurations used in this investigation gave Mach numbers of 1.64, 2.0, 2.55, and 3.0. At each Mach number the test-section density varies continuously to a controlled maximum.

Description of Models

The models simulated a delta-planform canard all-movable control surface. They were cut from 2024-T aluminum sheet stock, the thickness of a given model being constant over the planform except for the beveled leading and trailing edges. The geometry of the models and model-mount fairings is shown in figure 1. The portion of the mount fairings forward of the trailing edge represents the contour of a vehicle body.

The masses and thicknesses of the control-surface models, identified by numbers 1 to 9, are presented in table I. The method of mounting the models for use in both the 9- by 18-inch supersonic flutter tunnel and the 2-foot transonic flutter tunnel is shown in figures 2 and 3. The torque rod was connected to the mount frame through a torsional spring. Several torsion springs were used to cover a range of stiffnesses. Combinations of torsion springs and control-surface thickness were selected to produce symmetrical and antisymmetrical modes considered to be realistic for this type of control. These combinations are hereinafter referred to as basic combinations or the basic configuration. In addition, several modified combinations were used to increase the scope of the investigation. It should be noted that although the physical appearance of the model mounts was different, the model root conditions were the same in both mounts.

A model mounted in each of the tunnels is shown in figures 4 and 5. Also shown in figures 4 and 5 are the different mount fairings used in the two tunnels. The differences in model-mount fairings are also indicated in figure 1.

TABLE I

MASS AND THICKNESS OF MODELS

Model	Mass		Thickness	
	slugs	kg	in.	cm
1	0.000732	0.01068	0.016	0.0406
2	.000928	.01355	.020	.0508
3	.001446	.02111	.032	.0812
4	.001875	.02738	.040	.1016
5	.002371	.03461	.051	.1295
6	.002890	.04220	.064	.1626
7	.003095	.04520	.072	.1828
8	.003650	.05330	.080	.2033
9	.003895	.05710	.091	.2311

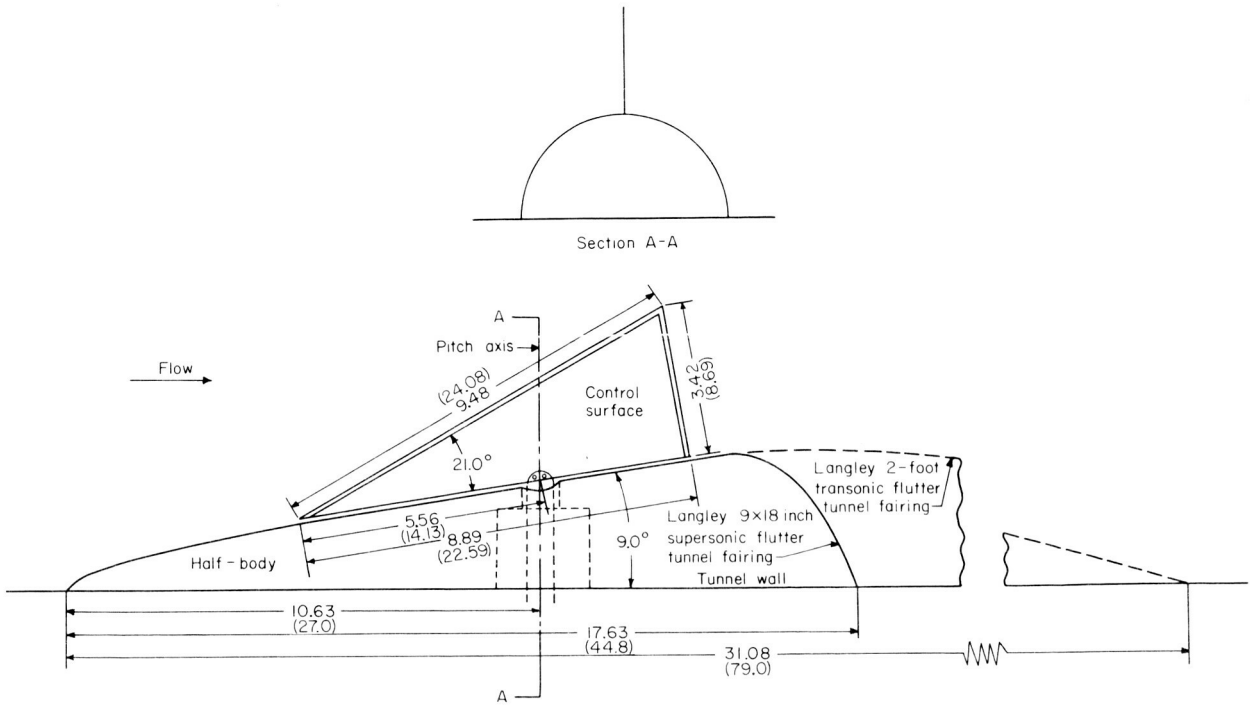

Figure 1.- Geometry of models and mount fairings. (Dimensions are shown in inches and parenthetically in centimeters.)

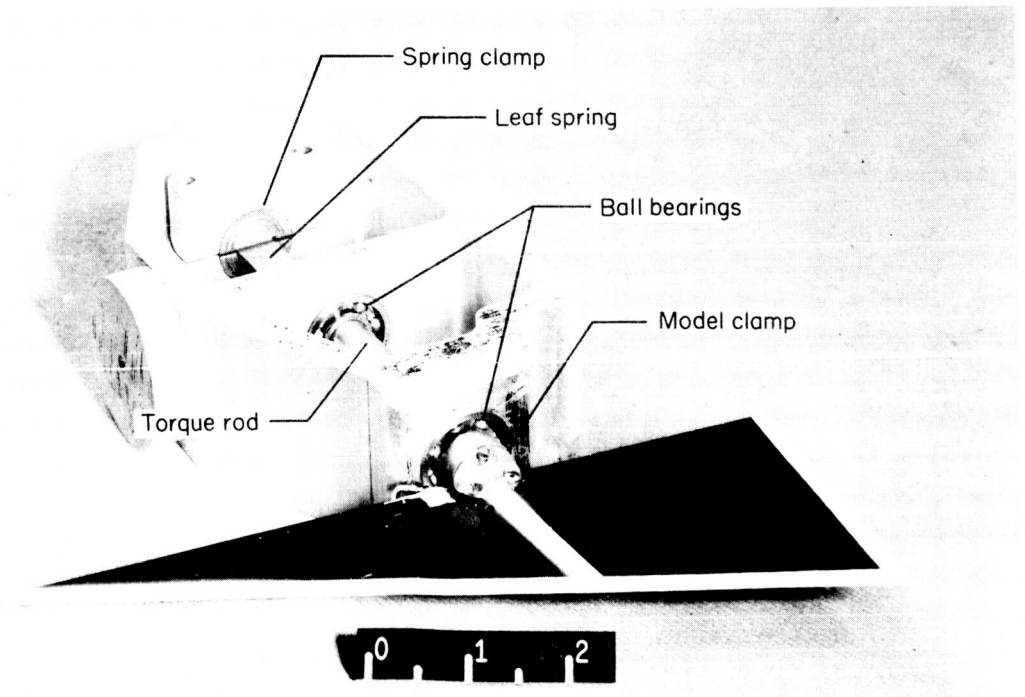

Figure 2.- Model mount used in the Langley 2-foot transonic flutter tunnel. (Scale shown is in inches.) L-57-1783.1

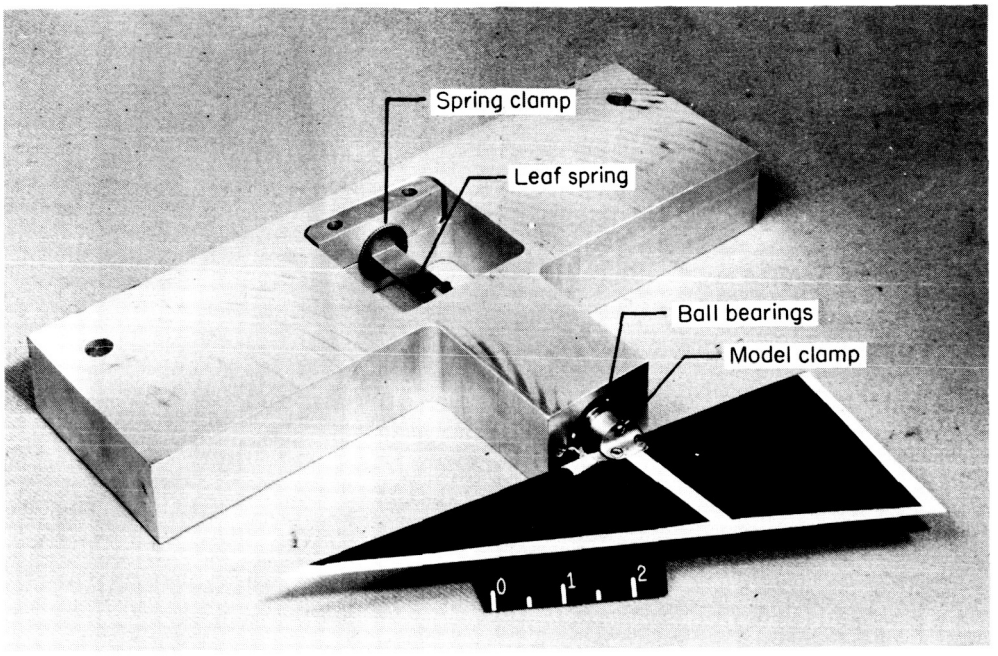

(a) View looking toward root. L-57-1782.1

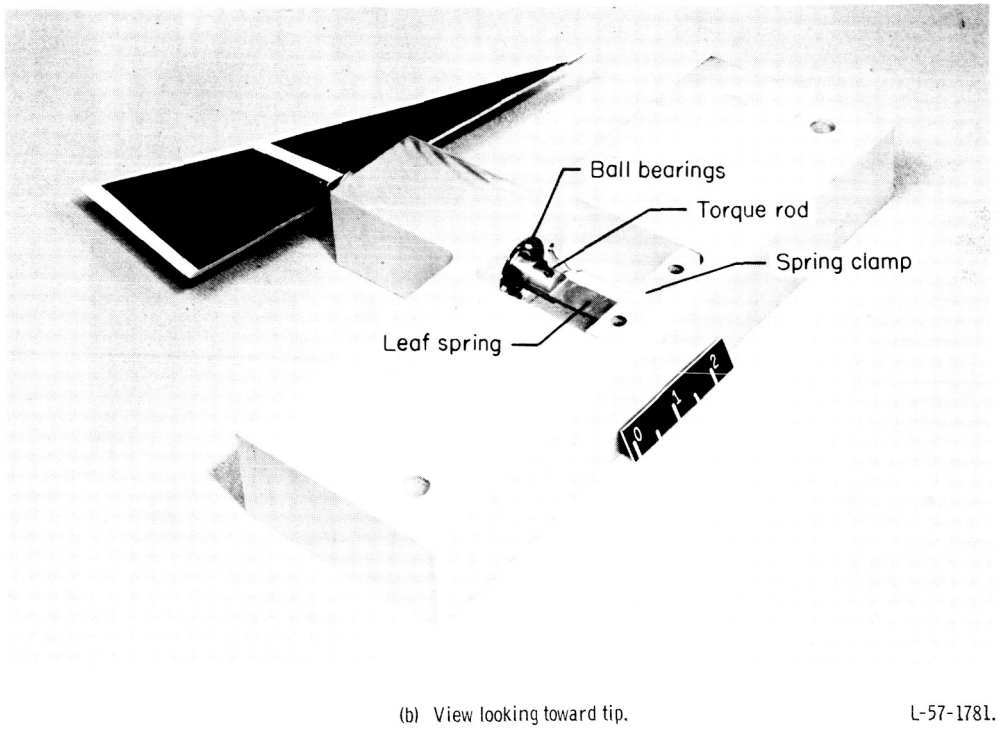

(b) View looking toward tip. L-57-1781.1

Figure 3.- Model mount used in the Langley 9- by 18-inch supersonic flutter tunnel. (Scale shown is in inches.)

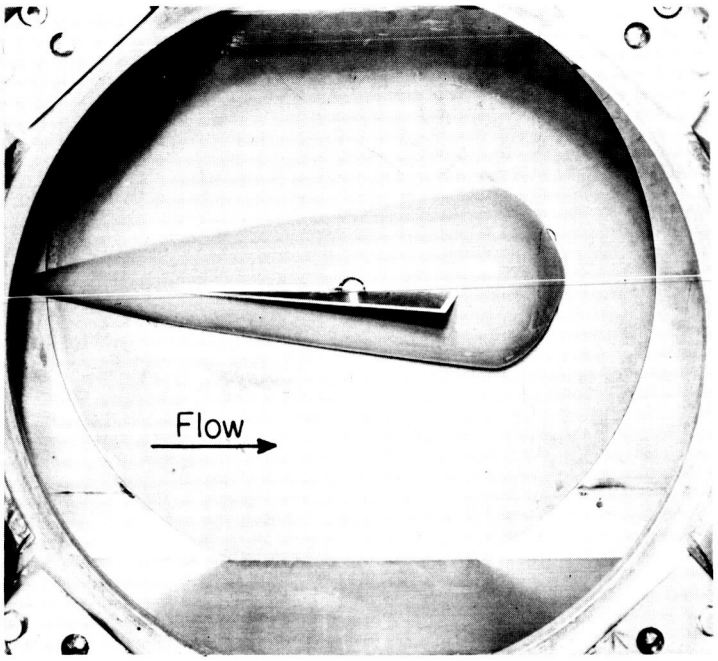

L-57-1437.1

Figure 4.- Model mounted in Langley 9- by 18-inch supersonic flutter tunnel.

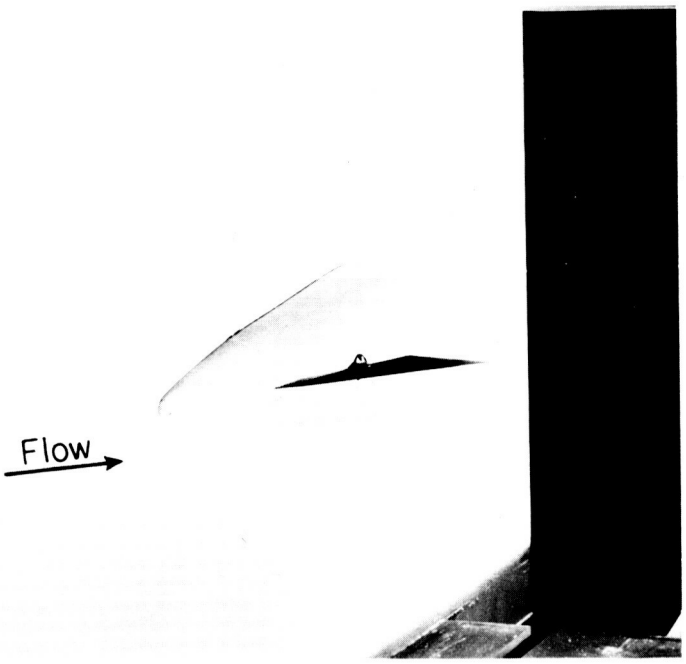

L-57-1430.1

Figure 5.- Model mounted in Langley 2-foot transonic flutter tunnel.

The torsional stiffness h of the springs is presented in table II, along with the control-surface-panel stiffness d and combination panel-spring stiffness K_e. The numbers of the control-surface model and the spring are used in the model designations in table II; thus, model 3-2 is control-surface model 3 mounted on spring 2. The column headed d is the measured deflection of the control surface at a point due to a unit load at that point with the pitch spring stiffness assumed infinite and the column headed h is the deflection of an infinitely stiff control surface at a point due to a unit load at that point acting against the pitch spring stiffness only. The point of reference is a point 27.1 percent of the root chord rearward of the leading edge and 50 percent of the local span outboard of the root chord. The effective stiffness K_e is a measure of the total stiffness of the model and is defined as $\frac{1}{d + h}$. Also shown in table II are calculated divergence dynamic pressures obtained from an analysis discussed subsequently.

TABLE II

STIFFNESS PROPERTIES OF MODELS AND SPRINGS WITH CALCULATED DIVERGENCE DYNAMIC PRESSURE

Models	d		h		K_e		Calculated divergence q (low-aspect-ratio theory)*	
	ft/lb	cm/N	ft/lb	cm/N	lb/ft	N/cm	lb/sq ft	N/cm^3
Basic control-surface—spring combinations								
3-2	0.01950	0.13360	0.03173	0.21730	19.51	2.85	82.60	0.39
4-3	.00925	.06340	.01417	.09710	42.70	6.23	168.00	.80
6-5	.00242	.01657	.00434	.02972	148.10	21.61	646.00	3.09
6-8	.00242	.01657	.00175	.01199	240.00	35.00	826.00	3.95
7-6	.00171	.01172	.00308	.02110	208.70	30.50	906.00	4.33
7-9	.00171	.01172	.00117	.00802	347.80	50.80	1,190.00	5.70
5-4	.00484	.03315	.00684	.04685	85.70	12.50	349.00	1.67
8-7	.00121	.00829	.00363	.02487	257.80	40.30	1,222.00	5.85
9-8	.00083	.00579	.00258	.01767	388.00	56.60	1,762.00	8.44
Modifed control-surface—spring combinations								
3-3	0.01950	0.13360	0.01417	0.09710	29.70	4.34	103.00	0.49
3-10	.01950	.13360	.00067	.00459	49.58	7.24	141.00	.68
9-2	.00083	.00579	.03173	.21730	30.68	4.48	652.00	3.12
3-1	.01950	.13360	.25500	1.74700	3.64	.53	41.70	.20
1-2	.15570	1.06700	.03173	.21730	5.34	.78	16.00	.08
2-2	.07980	.54700	.03173	.21730	8.98	1.31	28.60	.14
4-2	.00925	.06340	.03173	.21730	24.40	3.56	129.00	.62
5-2	.00484	.03315	.03173	.21730	27.40	4.00	208.00	1.00

*Divergence q calculated using piston theory is approximately equal to divergence q calculated using low-aspect-ratio theory multiplied by 0.906M.

Test Procedure

Langley 9- by 18-inch supersonic flutter tunnel.- The models tested in the Langley 9- by 18-inch supersonic flutter tunnel were all the basic configuration; that is, the spring and control-surface combinations were such that the elastic properties of an actual canard all-movable control were simulated, as was the location of the pitch axis (0.62 root chord). Electrical resistance wire strain gages were mounted at the root near the hinge line and the signal was taken to a recording oscillograph which also recorded tunnel conditions. In addition, high-speed motion-picture cameras recorded the behavior of the model. The procedure for making all the runs was as follows: the models were set at zero angle of attack and then the tunnel was evacuated to approximately 1 in. (2.54 cm) Hg absolute. A control valve upstream of the test section was then opened and the density of the flow was allowed to increase at constant Mach number until divergence occurred.

Langley 2-foot transonic flutter tunnel.- In addition to the basic configuration, several modified configurations were tested in the Langley 2-foot transonic flutter tunnel. Effects of variation of the pitch-axis location and of variations of spring and control-surface stiffnesses were investigated. In order to obtain data at various Mach numbers, the following procedure was used. With the tunnel set at a low density, the velocity was increased until the desired Mach number was reached. With the velocity held approximately constant, the test-section density was slowly increased until divergence occurred. The dynamic pressure was then decreased rapidly by actuating a spoiler in the diffuser section of the tunnel. The Mach number was then decreased to a point well below the divergence condition. At this point the stagnation pressure was increased by a small amount; the velocity was then slowly increased until divergence occurred. This procedure was repeated for several small increments in stagnation pressure. For the type of boundary found for these models, this procedure resulted in divergence points for several Mach numbers from the maximum obtainable in the tunnel down to some arbitrary lower Mach number.

Data Reduction

It was necessary to test models of different stiffnesses in order to obtain divergence data over the desired range of Mach number within the range of dynamic pressure obtainable in the test facilities. This variation in stiffness leads to the necessity of reducing the data obtained for the various models to some form of dimensionless parameter which will provide a basis for comparison of the test results at various Mach numbers. Such a parameter has been developed and discussed in appendix B. The parameter chosen is closely related to the stiffness-altitude parameter which has proven useful in interpreting flutter results. The divergence parameter differs from the flutter parameter in that the frequency and mass have been replaced by a stiffness term in an attempt to recognize the static characteristics of divergence.

This parameter is

$$\frac{b}{a}\sqrt{\frac{K_e}{m_A}}$$

where b is a reference semichord taken at the 75-percent-semispan station, a is the speed of sound, and K_e is the effective stiffness or the load required for a unit deflection measured at an arbitrary point on the surface. For all the models tested, b is 0.0926 foot (2.82 cm) and m_A is the mass of air which can be contained in a cone whose base diameter is equal to the root chord and whose height is equal to the exposed span of the control surface. The volume of this cone is 0.0405 cubic foot (1147 cm^3).

The results of the experiments are discussed subsequently, along with results obtained from the following analysis.

ANALYSIS

This section is concerned with the development of divergence equations applicable to the spring-mounted elastic control tested in the experimental investigation. An influence-coefficient method of analysis is used in which two methods are used for representing the aerodynamic forces, namely, low-aspect-ratio theory (ref. 3) and piston theory (ref. 4).

Structural Representation

In order to represent structurally the surface in a manner that is readily amenable to analysis, the sections of the surface were considered to be sheared parallel to the pitch axis and the trailing edge was rotated about its midspan point so that an equivalent symmetrical planform was obtained. The equivalent planform is indicated in the following sketch:

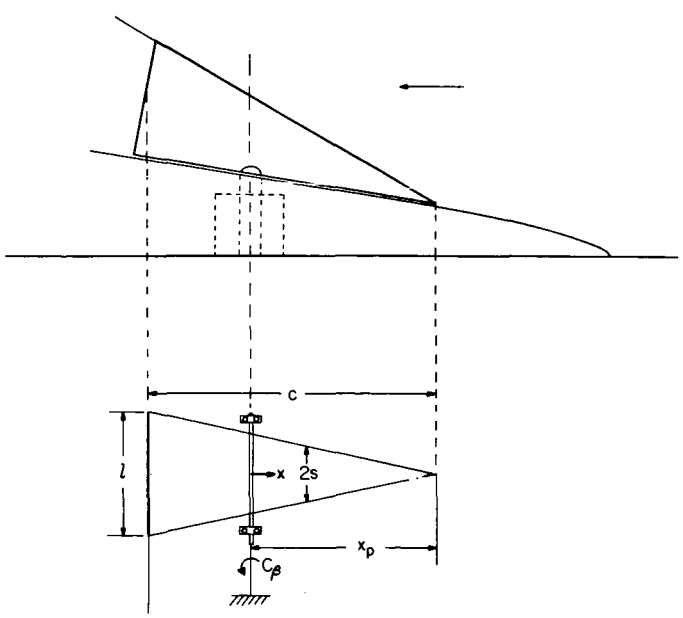

In both the low-aspect-ratio-theory and the piston-theory approaches, the aerodynamic loading is defined in terms of the local streamwise slopes and curvatures. The expressions for aerodynamic loading can be combined with the slope influence coefficients of the system to obtain an expression for the dynamic pressure at divergence. A first step in the development of the divergence equations is the determination of the combined slope influence coefficients of the spring-mounted elastic surface. The simple beam equation is applied

in the stream direction to determine a slope influence-coefficient array. It is assumed that the influence of spanwise deformations on the structural and aerodynamic forces is small. The elastic influence coefficients of the surface alone may be obtained by assuming that C_β, the pitch-spring constant, is infinitely stiff; that is, slope and deflection at the pitch axis are zero. Use may then be made of the fundamental beam relation

$$EI \frac{d^2z}{dx^2} = m_b \tag{1}$$

For a concentrated load P_{x_j} applied at a point at a distance x_j from the pitch axis, equation (1) becomes

$$EI \frac{d^2z}{dx^2} = -\left(x_j - x\right) P_{x_j} \tag{2}$$

for

$$|x| < |x_j|$$

Since the surfaces considered are of constant thickness, the section moment of inertia I may be written as

$$I = \frac{lt^3}{12c}\left(x_p - x\right) \tag{3}$$

Equation (2) may be integrated with the section moment of inertia represented by equation (3) to obtain the slope at a point x_i due to a load at station x_j:

$$\left(\frac{dz}{dx}\right)_{x_i} = \frac{12ncP_{x_j}}{Elt^3}\left[x_i - \left(x_p - x_j\right)\log_e \frac{x_p}{x_p - x_i}\right] \tag{4}$$

where

$$\left.\begin{aligned} n &= 1 \qquad \left(0 < x_i < x_j\right) \\ n &= 0 \qquad \left(x_j = 0\right) \\ n &= -1 \qquad \left(x_j < x_i < 0\right) \end{aligned}\right\} \tag{5a}$$

Appropriate boundary conditions are

$$\left.\begin{aligned} \left(\frac{dz}{dx}\right)_{x_i} &= \left(\frac{dz}{dx}\right)_{x_j} \qquad \left(|x_i| > |x_j|;\ x_i x_j > 0\right) \\ \left(\frac{dz}{dx}\right)_{x_i} &= 0 \qquad \left(x_i x_j \leqq 0\right) \end{aligned}\right\} \tag{5b}$$

An elastic slope influence coefficient A_{ij} may then be defined as

$$A_{ij} = \frac{\left(\frac{dz}{dx}\right)_{x_i}}{P_{x_j}} = \frac{12nc}{Elt^3} x_p \left[\frac{x_i}{x_p} - \left(1 - \frac{x_j}{x_p}\right) \log_e \frac{1}{1 - \frac{x_i}{x_p}} \right] \tag{6}$$

subject to the conditions of equations (5).

For the present analysis the control surface is divided into 10 sections of equal increments along x and the control points are located at the middle of each section. The 10-point slope influence coefficient matrix [A] calculated from equation (6) and representing the control surfaces is presented in appendix C.

The slope influence coefficient a_{ij} due to a spring in the pitch degree of freedom is

$$a_{ij} = \frac{x_j}{C_\beta} \tag{7}$$

The matrix [a] representing the influence coefficients for the pitch springs is also presented in appendix C.

The combined slope influence coefficients due to the elastic control surface and the spring restraint in the pitch degree of freedom are additive,

$$B_{ij} = A_{ij} + a_{ij} = [B] \tag{8}$$

The matrix equation

$$\left\{\frac{dz}{dx}\right\} = [B]\{P\} \tag{9}$$

gives the slope $\left\{\frac{dz}{dx}\right\}$ in the streamwise direction for any system of loads $\{P\}$. If the aerodynamic loads can be expressed in terms of the dynamic pressure and slope, substitution of the aerodynamic loads into equation (9) results in the divergence equations which may be iterated to obtain the critical dynamic pressure. Two methods of representing the aerodynamic loads are used, namely, low-aspect-ratio theory and piston theory. The following section presents the development of the aerodynamic loads into a form that can be used in equation (9) to obtain the divergence equation.

Divergence Equations

Low-aspect-ratio theory.- The aerodynamic loads are first obtained from very-low-aspect-ratio theory (ref. 3). This theory assumes that the flow field within a planar strip perpendicular to the flow direction is two dimensional

and that the changes in the flow direction are small. The complete expression for the aerodynamic load on a section of dimension $2s$ normal to the flow and Δx parallel to the flow may be written as

$$P = -\pi\rho(\Delta x)s^2\left(\ddot{z} + zV\frac{d\dot{z}}{dx} + V^2\frac{d^2z}{dx^2}\right) - 2\pi(\Delta x)\rho Vs\tan\theta\left(\dot{z} + V\frac{dz}{dx}\right) \tag{10}$$

where θ is the angle at which the leading edge is inclined to the free stream. The effects of the central body on the aerodynamic forces as given by low-aspect-ratio theory are not known; however, they are assumed to be small. The time derivatives for the divergence case vanish, and equation (10) when applied over the entire control surface may be written in matrix notation as

$$\{P\} = -2\pi(\Delta x)q\left\{\left[s^2\frac{d^2z}{dx^2}\right\} + 2\tan\theta\left\{s\frac{dz}{dx}\right]\right\} \tag{11}$$

If

$$\left.\begin{aligned}\delta_{ij} &= 1 \qquad (i = j)\\ \delta_{ij} &= 0 \qquad (i \neq j)\end{aligned}\right\} \tag{12}$$

the matrix for the aerodynamic loads becomes

$$\{P\} = 2\pi(\Delta x)q\left\{\left[\delta_{ij}s_j^2\right]\left\{\frac{d^2z}{dx^2}\right\} + 2\tan\theta\left[\delta_{ij}s_j\right]\left\{\frac{dz}{dx}\right\}\right\} \tag{13}$$

A differentiating matrix $[D]$ may be determined so that

$$\left\{\frac{d^2z}{dx^2}\right\} = [D]\left\{\frac{dz}{dx}\right\} \tag{14}$$

A sample matrix $[D]$ for the 10-point analysis used in this paper is given in appendix C. If the differentiating matrix $[D]$ of equation (14) is used in equation (13), the expression for the aerodynamic loads becomes

$$P = -2\pi(\Delta x)q\left[\left[\delta_{ij}s_j^2\right][D] + 2\tan\theta\left[\delta_{ij}s_j\right]\right]\left\{\frac{dz}{dx}\right\} \tag{15}$$

The square matrix premultiplying $\left\{\frac{dz}{dx}\right\}$ is a function of geometry only, and, if it is denoted by $[C]$, the aerodynamic loads are given by

$$\left\{P\right\} = -2\pi(\Delta x)q[C]\left\{\frac{dz}{dx}\right\} \tag{16}$$

If the aerodynamic loads given by equation (16) are substituted into the combined slope influence equation (eq. (9)), the equation governing the slopes under aerodynamic loadings is

$$\left\{\frac{dz}{dx}\right\} = -2\pi(\Delta x)q[B][C]\left\{\frac{dz}{dx}\right\} \tag{17}$$

Equation (17) expresses the conditions for which the aerodynamic forces are equal to the structural restoring forces. Equation (17) is thus the divergence equation and may be iterated to obtain the dominant root which yields the dynamic pressure at divergence. The values of q thus obtained for each case are given in table II. The product $[B]$ $[C]$ for stiff control surfaces and weak pitch springs produced an ill-conditioned matrix which was divergent under normal iteration procedures. Averaging successive iterations proved to be adequate to force convergence to the dominant mode in the cases treated.

Piston theory.- A second method of representing the aerodynamic forces for the supersonic case was also used and involved the use of piston theory (ref. 4). Piston theory is an application of the "local" wave equation and may be obtained from potential-flow theory if the Mach number is allowed to take on large values. The pressure coefficient may be written as

$$p - p_\infty = p_\infty a_\infty{}^2\left[\frac{w}{a_\infty} + \frac{\gamma + 1}{4}\left(\frac{w}{a_\infty}\right)^2 + \frac{\gamma + 1}{12}\left(\frac{w}{a_\infty}\right)^3 + \cdots\right] \tag{18}$$

The load on a section of the upper surface, which is $2s$ wide and Δx long, becomes

$$P_U = -2(\Delta x)(2s)q\left[\frac{1}{M}\frac{w}{V} + \frac{\gamma + 1}{4}\left(\frac{w}{V}\right)^2 + M^3\frac{\gamma + 1}{12}\left(\frac{w}{V}\right)^3 + \cdots\right] \tag{19}$$

The surface is of constant thickness and the load on a section of the lower surface is

$$P_L = -2(\Delta x)(2s)q\left[-\frac{1}{M}\frac{w}{V} + \frac{\gamma + 1}{4}\left(\frac{w}{V}\right)^2 - M^3\frac{\gamma + 1}{12}\left(\frac{w}{V}\right)^3 + \cdots\right] \tag{20}$$

If dz/dx is equal to w/V, the total load $P_U - P_L$ becomes

$$P = -4(\Delta x)(2s)q\left[\frac{1}{M}\frac{dz}{dx} + M^3\left(\frac{\gamma + 1}{12}\right)\left(\frac{dz}{dx}\right)^3 + \cdots\right] \tag{21}$$

Only the first term of equation (21) is used in the present analysis. The system of equations representing the loads on the control surface is

$$\left\{P\right\} = -\frac{4}{M}(\Delta x)q\left[2\delta_{ij}s_j\right]\left\{\frac{dz}{dx}\right\} \tag{22}$$

Equation (13) is the corresponding equation derived from low-aspect-ratio theory. The square matrix premultiplying $\left\{\frac{dz}{dx}\right\}$ in equation (22) is also a function of geometry only, and, if it is denoted by $[c]$, the aerodynamic loads are

$$\left\{P\right\} = -\frac{4}{M}(\Delta x)q[c]\left\{\frac{dz}{dx}\right\} \tag{23}$$

Substituting the aerodynamic loads given by equation (23) into equation (9) gives the divergence equation for the analysis based on piston theory

$$\left\{\frac{dz}{dx}\right\} = -\frac{4}{M}(\Delta x)q[B][c]\left\{\frac{dz}{dx}\right\} \tag{24}$$

Equation (24) may be iterated to obtain the critical values of q.

RESULTS AND DISCUSSION

The basic model configuration with springs which simulated representative symmetric and antisymmetric stiffnesses of a canard control has been tested in the two wind tunnels in the Mach number range from about $M = 0.6$ to $M = 3.0$. Additional tests have been made in the transonic tunnel to study the effects of stiffness of the control rotation springs and of the control surface and additional studies were made of the effects of location of the pitch axis.

General Characteristics of the Divergence Encountered

Classically, divergence has been treated as an aeroelastic phenomenon associated with torsional deformations. This type of divergence has been defined as a static instability of an airfoil in torsion which occurs when the torsional rigidity of the structure is exceeded by aerodynamic twisting moments (ref. 5). The type of divergence encountered in the present investigation seems to fit this same definition except that the role of torsional deformations has been replaced by camber deformations superimposed on a rotation of the control about its pitch axis. The type of motion involved is shown in figure 6 which is composed of enlargements from a high-speed motion picture. As the deflections become large, it can be seen that the surface has large curvature ahead of the pitch axis and a decided slope at the pitch axis. As a

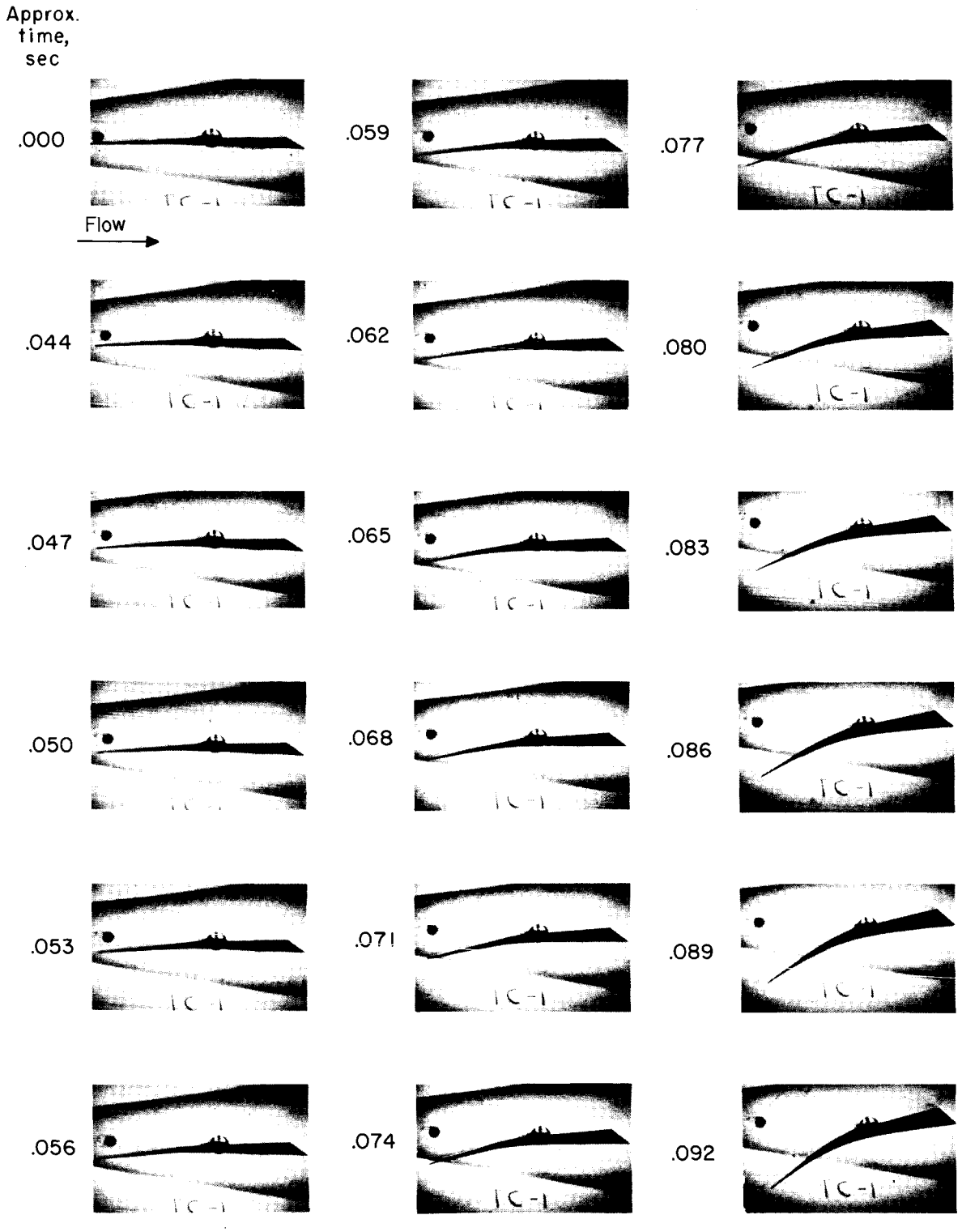

Figure 6.- Enlargements from high-speed motion picture of model 3-2 during divergence. L-58-1626

matter of interest, deflections were measured on several of the enlargements and are compared with the calculated deflection shape in figure 7. The agreement between the measured and calculated deflection shapes is good.

The type of motion involved in divergence of these models is very violent in the sense that very large deflections are reached in a very short period of time as indicated by the enlargements of the high-speed motion picture shown in figure 6. At subsonic and transonic speeds, only a few of the models acquired permanent set during divergence, presumably because of a stalling effect at high angles of attack. At supersonic speeds, all the models were permanently damaged in divergence. A representative selection of these damaged models is shown in figure 8. Although the models did not always suffer damage at the lower Mach numbers, the control deflections during divergence were probably sufficiently large to cause very violent maneuvers of a vehicle and subsequent structural damage.

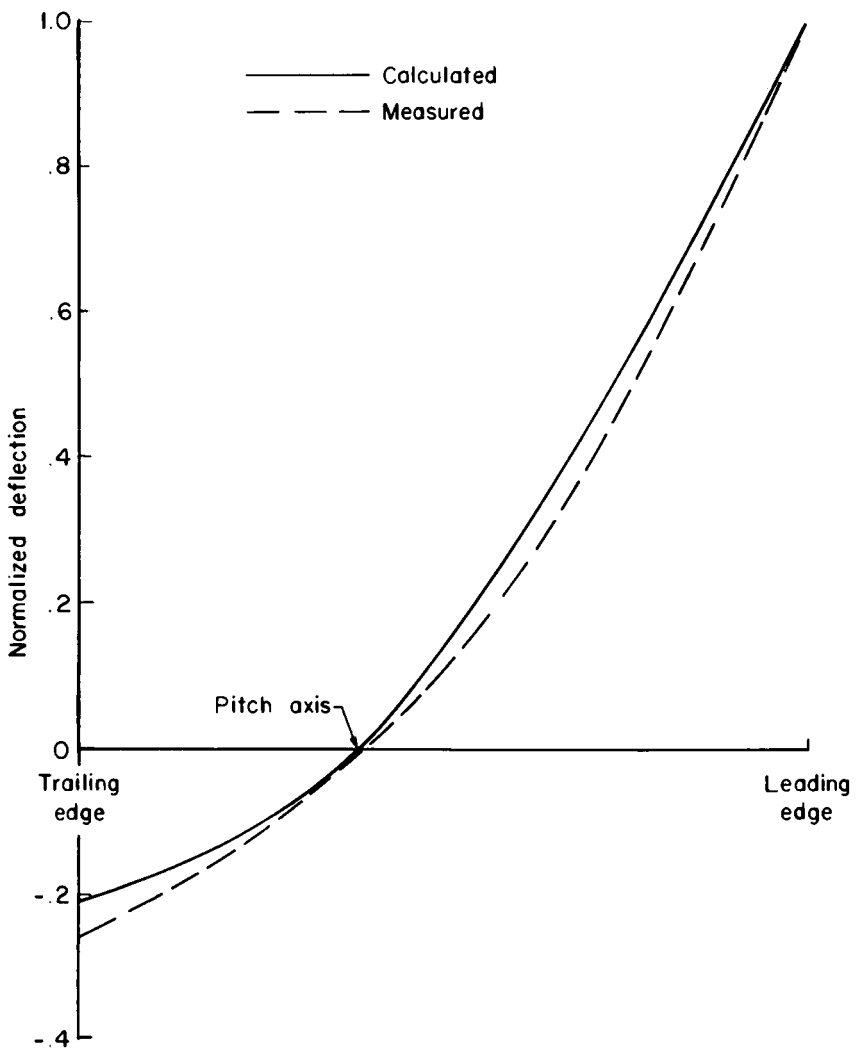

Figure 7.- Comparison of calculated and measured deflection modes during divergence.

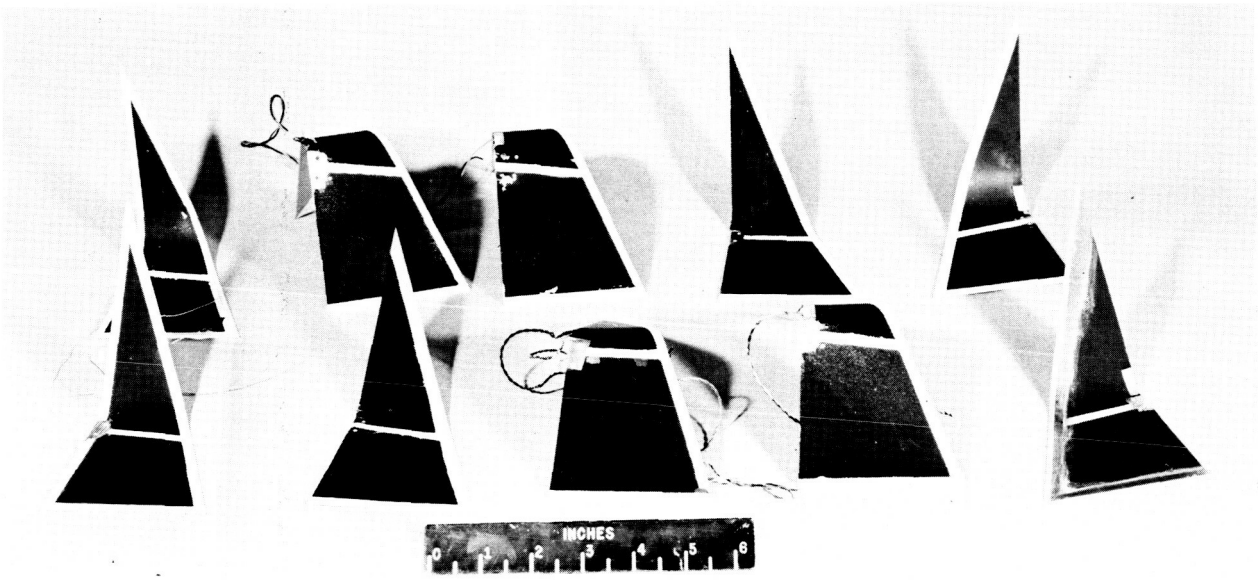

Figure 8.- Typical damaged models after supersonic testing. L-57-1438

Basic Configuration

The data obtained for the basic configuration have been reduced to a nondimensional stiffness-altitude parameter which is discussed in appendix A. The values of this parameter represent a stability boundary for static aeroelastic divergence and are shown as a function of Mach number in figures 9 and 10. In a figure of this type, constant-altitude operation of a given configuration would be represented by a horizontal line at a value of the parameter determined by the stiffness of the control and the altitude. Radial lines through the origin would represent lines of constant dynamic pressure.

The tendency toward a decrease in slope of the boundary with increasing Mach number indicates that somewhat higher dynamic pressures would be required to produce divergence at higher Mach numbers than at lower Mach numbers.

The analysis of static aeroelastic divergence using very-low-aspect-ratio aerodynamic theory yields a single value of dynamic pressure required to produce divergence regardless of the Mach number. If piston theory is used, the analysis indicates that the dynamic pressure at divergence increases directly with Mach number. The calculated results obtained from both types of aerodynamic theory are shown in figures 9 and 10. In the Mach number range from about 0.6 to 1.2 (where piston theory is not applicable), the agreement between the experiment and calculations based on low-aspect-ratio theory is considered to be excellent. At higher supersonic Mach numbers, the experimental results fall about one-half the distance between the calculated results obtained for the two types of aerodynamic theory. For clarity, the theoretical results are emphasized by the bands shown in figures 9 and 10.

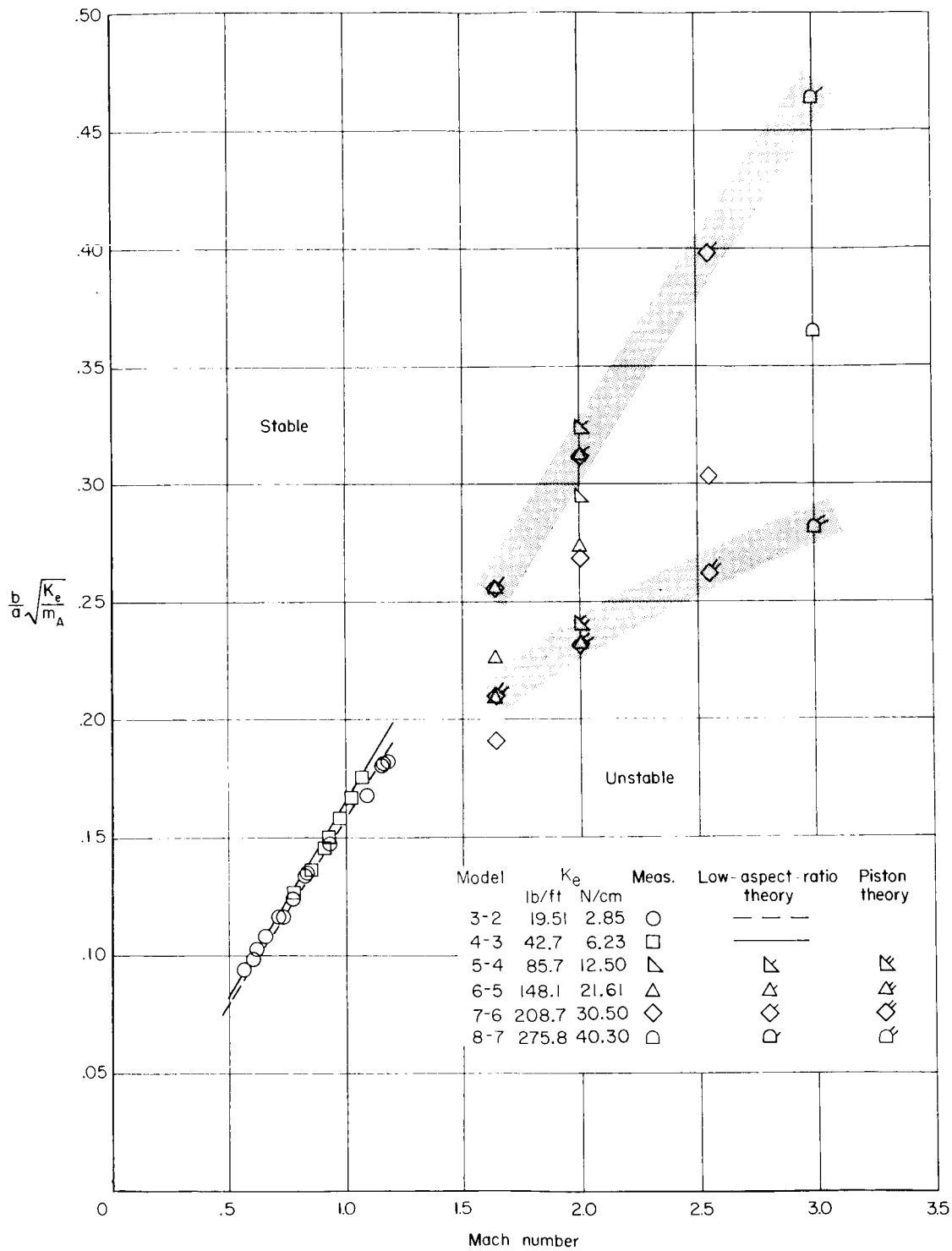

Figure 9.- Variation of stiffness-altitude divergence parameter with Mach number for models having springs simulating symmetric mode.

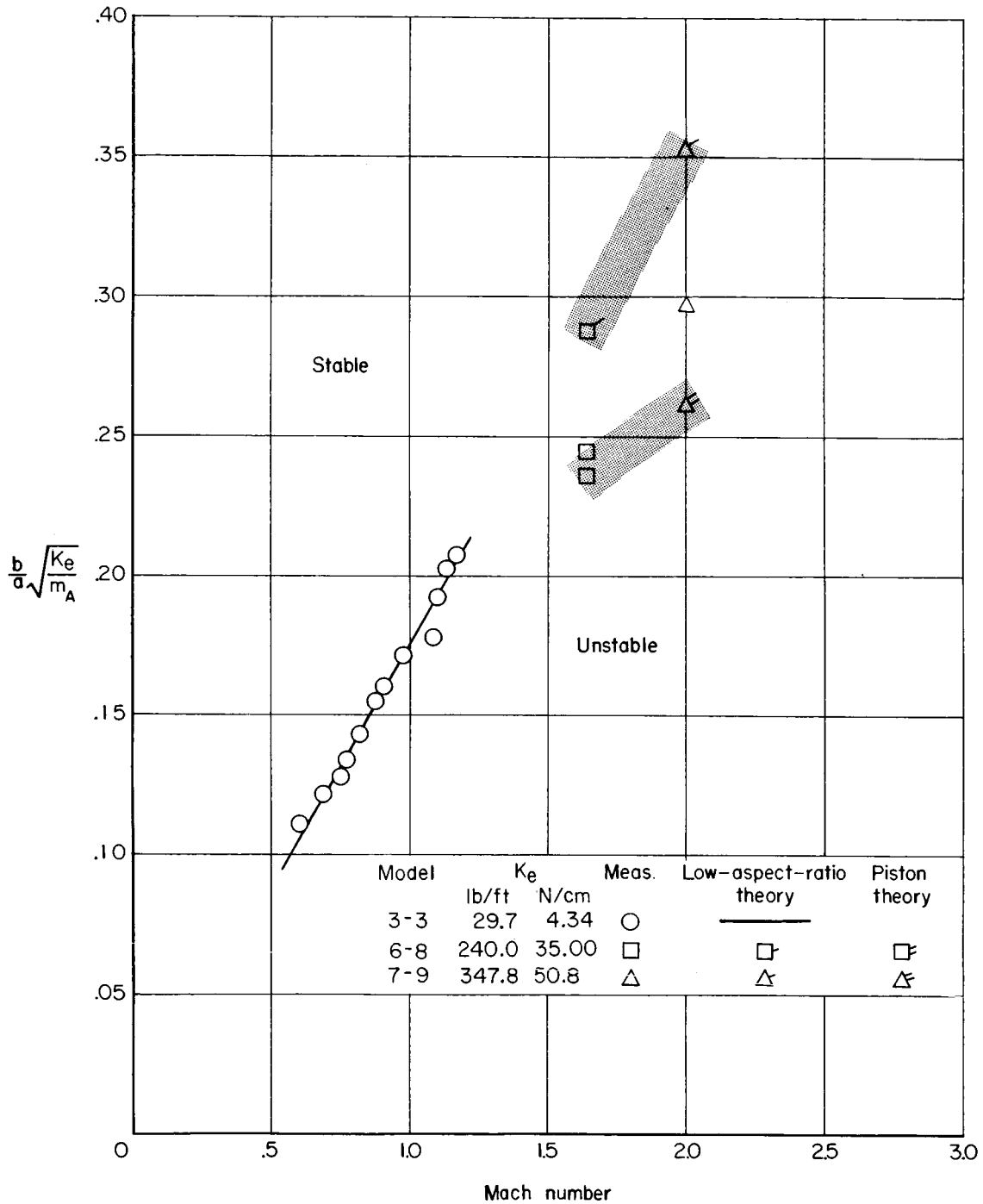

Figure 10.- Variation of stiffness-altitude divergence parameter with Mach number for models having springs simulating antisymmetric mode.

Effects of Variations in Stiffness

In order to obtain data over the desired range of Mach number in the two facilities, it was necessary to use models of varying stiffness. An impression of the effects of stiffness can be obtained by examining figures 9 and 10 and observing the degree to which a single curve can be fitted to the data for models of various stiffness levels. The fitting of a single straight line to the data implies that the dynamic pressure required for divergence is essentially directly proportional to the stiffness. This seems to be true for cases where the contributions of the control surface and the pitch spring to the total stiffness remain in about the same proportion. When the relative contributions of the two sources of stiffness are varied, this direct relationship between dynamic pressure and stiffness cannot be expected to apply. This feature is illustrated in figures 11 and 12, where the variation of the dynamic pressure required for divergence with stiffness is shown for two methods of varying the overall stiffness of the model. The first method (fig. 11) was to test the same control surface mounted on different springs simulating a variation in control actuator stiffness. The second method (fig. 12) was to test control surfaces of varying stiffness mounted on the same spring.

The data agree very well with the calculated values and indicate that the stiffness of the surface and the stiffness of the control actuator are both important in determining the divergence characteristics of controls of this type.

Effects of Variations of the Pitch Axis

It has long been recognized that the relative location of the aerodynamic center of pressure and the elastic axis is important in aeroelastic problems. In the present investigation it was believed that the camber deformations of the surface were producing a more forward location of the center of pressure than would be the case for a more rigid surface and, consequently, it was considered desirable to determine the effects of moving the elastic axis or the pitch axis forward. For a model with a particular stiffness of both the surface and the actuator, it was found that moving the pitch axis forward from 0.62c to 0.58c increased the dynamic pressure at divergence by about 35 percent. Similar tests with a much lower simulated actuator stiffness indicated about an 80-percent increase in dynamic pressure for the same change in axis location. When the same control surface was tested with the axis at midchord and with zero actuator stiffness (free floating), the dynamic pressure at divergence was increased by about 20 percent and thus indicated the strong influence of the location of the pitch axis.

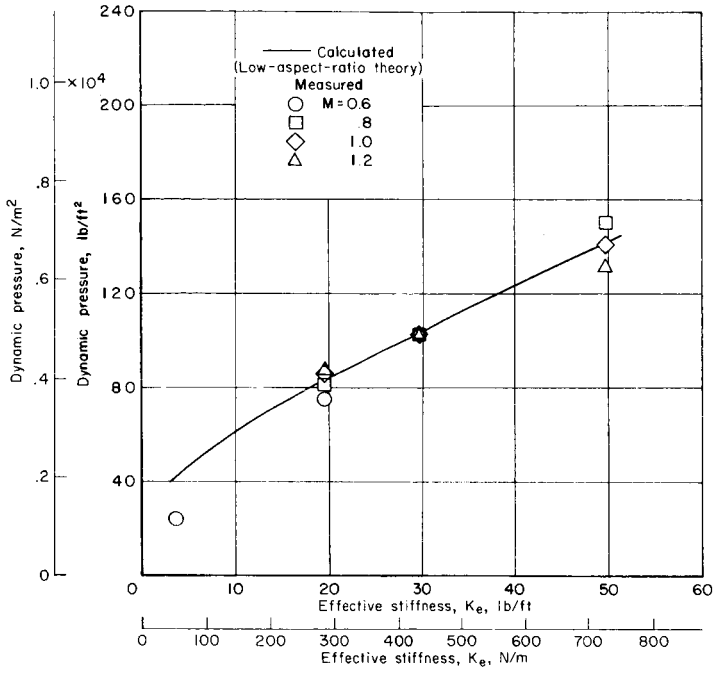

Figure 11.- Variation of dynamic pressure at divergence with stiffness for model 3 with various springs.

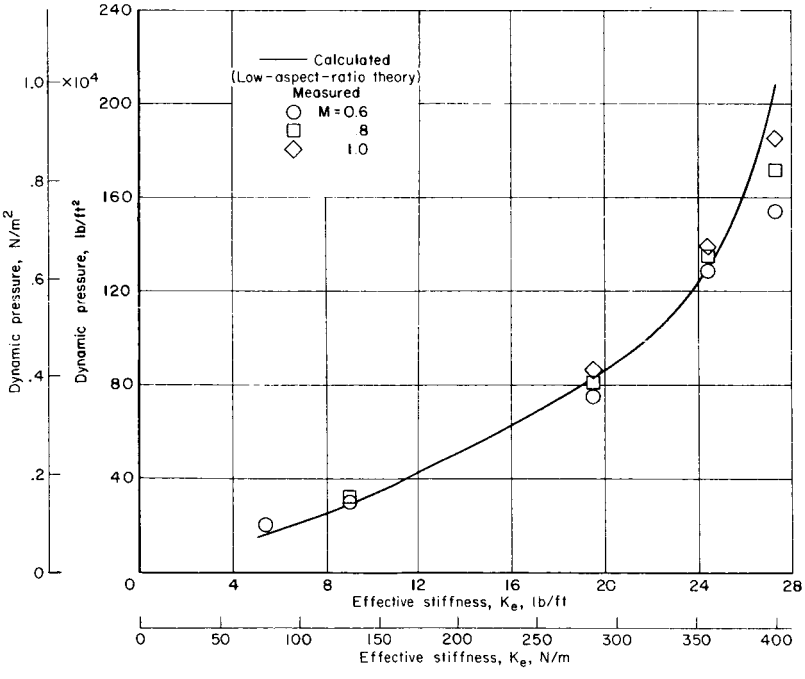

Figure 12.- Variation of dynamic pressure at divergence with stiffness for spring 2 with various models.

CONCLUSIONS

Divergence studies of a delta-planform all-movable canard control in the Mach number range from 0.6 to 3.0 indicate the following conclusions:

1. At Mach numbers from 0.6 to 1.2, divergence occurs at an almost constant value of dynamic pressure. At higher supersonic speeds up to a Mach number of 3.0, divergence occurs at somewhat higher values of dynamic pressure.

2. Analytical results based on very-low-aspect-ratio aerodynamic theory gave very good agreement with the experimental results in the Mach number range from 0.6 to 1.2. At higher Mach numbers, the experimental results fell about one-half the distance between two sets of calculated results based on low-aspect-ratio theory and piston theory.

3. The analysis and the experiment indicate that the stiffness of the control surface and the stiffness of the control actuator are both important in divergence of controls of this type.

Langley Research Center,
National Aeronautics and Space Administration,
Langley Station, Hampton, Va., April 14, 1958.

APPENDIX A

CONVERSION OF U.S. CUSTOMARY UNITS TO SI UNITS

The International System of Units was adopted by the Eleventh General Conference on Weights and Measures, Paris, October 1960. (See ref. 7.) Factors required for converting the U.S. Customary Units used herein to the International System of Units (SI) are given in the following table:

Physical quantity	U.S. Customary Unit	Conversion factor (*)	SI Unit
Force	lb	4.448	newtons (N)
Length	in.	0.0254	meters (m)
	ft	0.3048	meters (m)
Mass	slugs	14.59	kilogram (kg)
Pressure	lb/sq in.	6895	newtons/meter^2 (N/m^2)
	lb/sq ft	47.88	newtons/meter^2 (N/m^2)
Volume	cu ft	0.0283	meters (m^3)

*Multiply value given in U.S. Customary Unit by conversion factor to obtain equivalent value in SI unit.

Prefixes to indicate multiples of units are as follows:

Prefix	Multiple
centi (c)	10^{-2}
kilo (k)	10^3

APPENDIX B

DERIVATION OF A PARAMETER FOR PRESENTATION OF EXPERIMENTAL DIVERGENCE DATA

In the study of dynamic aeroelastic phenomena or flutter, a convenient grouping of parameters called the stiffness-altitude parameter has been very useful in interpreting experimental flutter data obtained for a variety of stiffnesses over a range of altitude and Mach number. This flutter parameter consists of the product of a reduced frequency based on a representative chord, natural frequency, and the speed of sound times the square root of a mass ratio which is usually taken as the ratio of the mass of the surface to the mass of a specified volume of air surrounding the surface. This flutter parameter can be written as $\frac{b\omega}{a}\sqrt{\mu}$.

If it is reasoned that static aeroelastic phenomena, in particular divergence, do not depend on inertia forces, it seems logical that some other combination of parameters might be more useful in interpreting divergence data. If the divergence model can be represented by a concentrated mass which yields the frequency ω when attached to a spring with a spring constant K_e, the flutter parameter might be redefined as

$$\frac{b\omega}{a}\sqrt{\mu} = \frac{b\sqrt{\frac{K_e}{m_e}}}{a}\sqrt{\frac{m_e}{m_A}} = \frac{b}{a}\sqrt{\frac{K_e}{m_A}}$$

This new parameter would seem to be more appropriate for divergence studies since it is not based on dynamic properties of the model but does include the stiffness of the surface. However, the new parameter is somewhat unsatisfactory because the significance of the individual parts of the parameter is not obvious. As a matter of interest, the parameter can be reduced further to

$$\frac{b}{a}\sqrt{\frac{K_e}{m_A}} \approx \frac{b}{a}\sqrt{\frac{K_e}{\rho b^2 l}} \approx \frac{1}{a}\sqrt{\frac{K_e}{\rho l}}$$

where the product $\rho b^2 l$ is proportional to the mass of a particular volume of air surrounding the surface. The speed of sound can be eliminated by the relationship $a = \sqrt{\frac{E_A}{\rho}}$ where E_A is the modulus of elasticity of the medium. If

it is recognized that the spring constant K_e is proportional to an effective value of the modulus of elasticity of the material $E_{M,e}$, the parameter becomes

$$\frac{b}{a}\sqrt{\frac{K_e}{m_A}} \approx C\sqrt{\frac{E_{M,e}}{E_A}}$$

where C is a constant for a given configuration depending only on the geometry of the configuration. Thus, it is seen that the divergence parameter is, essentially, the ratio of the model stiffness to the air stiffness which would seem to be a very significant parameter.

The divergence boundary defined by the dimensionless stiffness-altitude parameter can be converted easily to a boundary in terms of dynamic pressure and Mach number for a particular configuration. At each point on the boundary the dynamic pressure at divergence can be found from the following relation:

$$q = \left(\frac{b^2 K_e}{2\frac{m_A}{\rho}}\right)\frac{M^2}{\left(\frac{b}{a}\sqrt{\frac{K_e}{m_A}}\right)^2}$$

where $\frac{m_A}{\rho}$ is the specified volume of the medium surrounding the surface.

APPENDIX C

SAMPLE DIVERGENCE CALCULATION

Presented in this appendix is a sample calculation of the dynamic pressure at divergence based on low-aspect-ratio theory. The dimensions are given for the equivalent control surface after the sections were sheared parallel to the pitch axis and adjusted to obtain a symmetrical control surface. The numerical example is given in the U.S. Customary Units. The control surface was represented by the following parameters:

$$E = 10\ 000\ 000 \text{ lb/sq in.} = 6\ 890\ 000 \text{ N/cm}^2$$

$$c = 8.55 \text{ in.} = 21.73 \text{ cm}$$

$$l = 3.60 \text{ in.} = 9.15 \text{ cm}$$

$$x_p = 5.45 \text{ in.} = 13.85 \text{ cm}$$

$$\Delta x = 0.855 \text{ in.} = 2.173 \text{ cm}$$

$$t = 0.032 \text{ in.} = 0.0813 \text{ cm}$$

$$1/C_\beta = 0.0345 \text{ radian/in-lb} = 0.00305 \text{ radian/cm-N}$$

$$\theta = 30^\circ = 0.524 \text{ radian}$$

The slope-influence-coefficient matrix for all the control surfaces, calculated from equation (6), is

$$\left[A_{ij}\right] = \frac{12c}{Elt^3}\begin{bmatrix} 3.937 & 2.320 & 1.323 & 0.674 & 0.271 & 0.058 & 0 & 0 & 0 & 0 \\ 3.554 & 2.320 & 1.323 & .674 & .271 & .058 & 0 & 0 & 0 & 0 \\ 2.922 & 2.122 & 1.323 & .674 & .271 & .058 & 0 & 0 & 0 & 0 \\ 2.216 & 1.702 & 1.188 & .674 & .271 & .058 & 0 & 0 & 0 & 0 \\ 1.475 & 1.174 & .873 & .572 & .271 & .058 & 0 & 0 & 0 & 0 \\ .711 & .580 & .450 & .319 & .189 & .058 & 0 & 0 & 0 & 0 \\ 0 & 0 & 0 & 0 & 0 & 0 & -.003 & -.018 & -.023 & -.034 \\ 0 & 0 & 0 & 0 & 0 & 0 & -.003 & -.074 & -.207 & -.339 \\ 0 & 0 & 0 & 0 & 0 & 0 & -.003 & -.074 & -.261 & -.500 \\ 0 & 0 & 0 & 0 & 0 & 0 & -.003 & -.074 & -.261 & -.548 \end{bmatrix} \qquad \text{(C1)}$$

The slope-influence-coefficient matrix for the pitch degree of freedom is given as

$$\left[a_{ij}\right] = \frac{1}{C_\beta}\begin{bmatrix} 5.019 & 4.170 & 3.322 & 2.473 & 1.625 & 0.776 & -0.072 & -0.921 & -1.769 & -2.618 \\ 5.019 & 4.170 & 3.322 & 2.473 & 1.625 & .776 & -.072 & -.921 & -1.769 & -2.618 \\ 5.019 & 4.170 & 3.322 & 2.473 & 1.625 & .776 & -.072 & -.921 & -1.769 & -2.618 \\ 5.019 & 4.170 & 3.322 & 2.473 & 1.625 & .776 & -.072 & -.921 & -1.769 & -2.618 \\ 5.019 & 4.170 & 3.322 & 2.473 & 1.625 & .776 & -.072 & -.921 & -1.769 & -2.618 \\ 5.019 & 4.170 & 3.322 & 2.473 & 1.625 & .776 & -.072 & -.921 & -1.769 & -2.618 \\ 5.019 & 4.170 & 3.322 & 2.473 & 1.625 & .776 & -.072 & -.921 & -1.769 & -2.618 \\ 5.019 & 4.170 & 3.322 & 2.473 & 1.625 & .776 & -.072 & -.921 & -1.769 & -2.618 \\ 5.019 & 4.170 & 3.322 & 2.473 & 1.625 & .776 & -.072 & -.921 & -1.769 & -2.618 \\ 5.019 & 4.170 & 3.322 & 2.473 & 1.625 & .776 & -.072 & -.921 & -1.769 & -2.618 \end{bmatrix} \qquad \text{(C2)}$$

APPENDIX C

The combined slope-influence-coefficient matrix $B_{ij} = A_{ij} + a_{ij}$ is obtained by adding equations (C1) and (C2):

$$[B_{ij}] = \begin{bmatrix} 0.513 & 0.344 & 0.229 & 0.144 & 0.080 & 0.032 & -0.003 & -0.032 & -0.061 & -0.090 \\ .480 & .344 & .229 & .144 & .080 & .032 & -.003 & -.032 & -.061 & -.090 \\ .425 & .327 & .229 & .144 & .080 & .032 & -.003 & -.032 & -.061 & -.090 \\ .364 & .291 & .217 & .144 & .080 & .032 & -.003 & -.032 & -.061 & -.090 \\ .300 & .245 & .190 & .135 & .080 & .032 & -.003 & -.032 & -.061 & -.090 \\ .235 & .194 & .153 & .113 & .072 & .032 & -.003 & -.032 & -.061 & -.090 \\ .173 & .144 & .115 & .085 & .056 & .027 & -.004 & -.033 & -.063 & -.093 \\ .173 & .144 & .115 & .085 & .056 & .027 & -.004 & -.038 & -.079 & -.119 \\ .173 & .144 & .115 & .085 & .056 & .027 & -.004 & -.038 & -.084 & -.133 \\ .173 & .144 & .115 & .085 & .056 & .027 & -.004 & -.038 & -.048 & -.138 \end{bmatrix} \quad (C3)$$

A differentiating matrix is obtained by applying the 5-point interpolation equations given on page 97 of reference 6:

$$[D] = \frac{1}{12(\Delta x)} \begin{bmatrix} 25 & -48 & 36 & -16 & 3 & 0 & 0 & 0 & 0 & 0 \\ 3 & 10 & -18 & 6 & -1 & 0 & 0 & 0 & 0 & 0 \\ -1 & 8 & 0 & -8 & 1 & 0 & 0 & 0 & 0 & 0 \\ 0 & -1 & 8 & 0 & -8 & 1 & 0 & 0 & 0 & 0 \\ 0 & 0 & -1 & 8 & 0 & -8 & 1 & 0 & 0 & 0 \\ 0 & 0 & 0 & -1 & 8 & 0 & -8 & 1 & 0 & 0 \\ 0 & 0 & 0 & 0 & -1 & 8 & 0 & -8 & 1 & 0 \\ 0 & 0 & 0 & 0 & 0 & -1 & 8 & 0 & -8 & 1 \\ 0 & 0 & 0 & 0 & 0 & 1 & -6 & 18 & -10 & -3 \\ 0 & 0 & 0 & 0 & 0 & -3 & 16 & -36 & 48 & -25 \end{bmatrix} \quad (C4)$$

The matrix $[\delta_{ij}s_j]$ is obtained from the geometry of the control and is expressed in inches as follows:

$$[\delta_{ij}s_j] = \left(\frac{3.6}{40}\right) \begin{bmatrix} 1 & 0 & 0 & 0 & 0 & 0 & 0 & 0 & 0 & 0 \\ 0 & 3 & 0 & 0 & 0 & 0 & 0 & 0 & 0 & 0 \\ 0 & 0 & 5 & 0 & 0 & 0 & 0 & 0 & 0 & 0 \\ 0 & 0 & 0 & 7 & 0 & 0 & 0 & 0 & 0 & 0 \\ 0 & 0 & 0 & 0 & 9 & 0 & 0 & 0 & 0 & 0 \\ 0 & 0 & 0 & 0 & 0 & 11 & 0 & 0 & 0 & 0 \\ 0 & 0 & 0 & 0 & 0 & 0 & 13 & 0 & 0 & 0 \\ 0 & 0 & 0 & 0 & 0 & 0 & 0 & 15 & 0 & 0 \\ 0 & 0 & 0 & 0 & 0 & 0 & 0 & 0 & 17 & 0 \\ 0 & 0 & 0 & 0 & 0 & 0 & 0 & 0 & 0 & 19 \end{bmatrix} \quad (C5)$$

and

APPENDIX C

$$\left[\delta_{ij}s_j\right]^2 = \left(\frac{3.6}{40}\right)^2 \begin{bmatrix} 1 & 0 & 0 & 0 & 0 & 0 & 0 & 0 & 0 & 0 \\ 0 & 9 & 0 & 0 & 0 & 0 & 0 & 0 & 0 & 0 \\ 0 & 0 & 25 & 0 & 0 & 0 & 0 & 0 & 0 & 0 \\ 0 & 0 & 0 & 49 & 0 & 0 & 0 & 0 & 0 & 0 \\ 0 & 0 & 0 & 0 & 81 & 0 & 0 & 0 & 0 & 0 \\ 0 & 0 & 0 & 0 & 0 & 121 & 0 & 0 & 0 & 0 \\ 0 & 0 & 0 & 0 & 0 & 0 & 169 & 0 & 0 & 0 \\ 0 & 0 & 0 & 0 & 0 & 0 & 0 & 225 & 0 & 0 \\ 0 & 0 & 0 & 0 & 0 & 0 & 0 & 0 & 289 & 0 \\ 0 & 0 & 0 & 0 & 0 & 0 & 0 & 0 & 0 & 361 \end{bmatrix} \tag{C6}$$

The matrix $[C]$ as obtained from equation (15) is

$$[C] = \left[\delta_{ij}s_j^2\right][D] + 2\tan\theta\left[\delta_{ij}s_j\right] \tag{C7}$$

and may be written

$$[C] = - \begin{bmatrix} 0.084 & 0.038 & -0.029 & 0.013 & -0.002 & 0 & 0 & 0 & 0 & 0 \\ -.021 & .240 & .129 & -.043 & .007 & 0 & 0 & 0 & 0 & 0 \\ .020 & -.159 & .519 & .159 & -.020 & 0 & 0 & 0 & 0 & 0 \\ 0 & .039 & -.312 & .727 & .312 & -.039 & 0 & 0 & 0 & 0 \\ 0 & 0 & .064 & -.516 & .935 & .516 & -.064 & 0 & 0 & 0 \\ 0 & 0 & 0 & .096 & -.770 & 1.142 & .770 & -.096 & 0 & 0 \\ 0 & 0 & 0 & 0 & .134 & -1.076 & 1.350 & 1.076 & -.134 & 0 \\ 0 & 0 & 0 & 0 & 0 & .179 & -1.432 & 1.558 & 1.432 & -.179 \\ 0 & 0 & 0 & 0 & 0 & -.230 & 1.379 & -4.138 & 4.065 & .690 \\ 0 & 0 & 0 & 0 & 0 & .862 & -4.595 & 10.338 & -13.785 & 9.153 \end{bmatrix} \tag{C8}$$

The product $[B][C]$ for use in equation (17) is found to be

$$[B][C] = - \begin{bmatrix} 0.040 & 0.071 & 0.109 & 0.095 & 0.091 & 0.005 & 0.392 & -0.736 & 0.952 & -0.863 \\ .037 & .070 & .110 & .094 & .091 & .005 & .392 & -.736 & .952 & -.865 \\ .033 & .064 & .110 & .094 & .091 & .005 & .392 & -.736 & .952 & -.863 \\ .029 & .055 & .100 & .093 & .091 & .005 & .392 & -.736 & .952 & -.865 \\ .024 & .045 & .085 & .084 & .089 & .005 & .392 & -.736 & .952 & -.863 \\ .019 & .035 & .067 & .067 & .076 & .002 & .393 & -.736 & .952 & -.863 \\ .014 & .026 & .050 & .050 & .056 & -.013 & .402 & -.760 & .983 & -.891 \\ .014 & .026 & .050 & .050 & .056 & -.033 & .509 & -.975 & 1.274 & -1.142 \\ .014 & .026 & .050 & .050 & .056 & -.044 & .566 & -1.099 & 1.446 & -1.272 \\ .014 & .026 & .050 & .050 & .056 & -.047 & .585 & -1.141 & 1.503 & -1.310 \end{bmatrix} \tag{C9}$$

The dominant root of this matrix is found by iteration and is equal to -0.327. The normalized slope mode is given by

APPENDIX C

$$\left\{\frac{dz}{dx}\right\} = \begin{Bmatrix} 1.000 \\ .989 \\ .962 \\ .888 \\ .761 \\ .575 \\ .347 \\ .275 \\ .240 \\ .233 \end{Bmatrix} \tag{C10}$$

The divergence dynamic pressure is given as

$$q = -\frac{1}{2\pi(\Delta x)(-0.327)} = 0.57 \text{ lb/sq in.} = 82 \text{ lb/sq ft} = 0.393 \text{ N/cm}^2$$

REFERENCES

1. Diederich, Franklin W.: Divergence of Delta and Swept Surfaces in the Transonic and Supersonic Speed Ranges. AGARD Rept. 42, Apr. 1956.

2. Biot, M. A.: The Divergence of Supersonic Wings Including Chordwise Bending. J. Aeron. Sci., vol. 23, no. 3, Mar. 1956, pp. 237-251.

3. Garrick, I. E.: Some Research on High-Speed Flutter. Third Anglo-American Aeronautical Conference (Brighton, England), Royal Aeron. Soc., 1952, pp. 419-446J.

4. Ashley, Holt; and Zartarian, Garabed: Piston Theory - A New Aerodynamic Tool for the Aeroelastician. J. Aeron. Sci., vol. 23, no. 12, Dec. 1956, pp. 1109-1118.

5. Scanlan, Robert H.; and Rosenbaum, Robert: Introduction to the Study of Aircraft Vibration and Flutter. The Macmillan Co., 1951.

6. Milne, William Edmund: Numerical Calculus. Princeton Univ. Press, 1949.

7. Mechtly, E. A.: The International System of Units - Physical Constants and Conversion Factors. NASA SP-7012, 1964.

NASA-Langley, 1966 L-4798

"The aeronautical and space activities of the United States shall be conducted so as to contribute . . . to the expansion of human knowledge of phenomena in the atmosphere and space. The Administration shall provide for the widest practicable and appropriate dissemination of information concerning its activities and the results thereof."

—NATIONAL AERONAUTICS AND SPACE ACT OF 1958

NASA SCIENTIFIC AND TECHNICAL PUBLICATIONS

TECHNICAL REPORTS: Scientific and technical information considered important, complete, and a lasting contribution to existing knowledge.

TECHNICAL NOTES: Information less broad in scope but nevertheless of importance as a contribution to existing knowledge.

TECHNICAL MEMORANDUMS: Information receiving limited distribution because of preliminary data, security classification, or other reasons.

CONTRACTOR REPORTS: Technical information generated in connection with a NASA contract or grant and released under NASA auspices.

TECHNICAL TRANSLATIONS: Information published in a foreign language considered to merit NASA distribution in English.

TECHNICAL REPRINTS: Information derived from NASA activities and initially published in the form of journal articles.

SPECIAL PUBLICATIONS: Information derived from or of value to NASA activities but not necessarily reporting the results of individual NASA-programmed scientific efforts. Publications include conference proceedings, monographs, data compilations, handbooks, sourcebooks, and special bibliographies.

Details on the availability of these publications may be obtained from:

SCIENTIFIC AND TECHNICAL INFORMATION DIVISION

NATIONAL AERONAUTICS AND SPACE ADMINISTRATION

Washington, D.C. 20546